Non-Maxwellian distribution in linear systems and its applications

Fernando Humire (f.humire@academicos.uta.cl)
Universidad de Tarapacá https://orcid.org/0000-0002-8054-3149
Rolando Caicedo
Universidade Estadual de Campinas Faculdade de Engenharia Eletrica e de Computacao
Ernesto Ruppert Filho
Universidade Estadual de Campinas Faculdade de Engenharia Eletrica e de Computacao
Mónica García–Ñustes
Pontificia Universidad Católica de Valparaíso: Pontificia Universidad Catolica de Valparaiso

Research Article

Keywords: Non-Maxwellian distribution, Asymmetric dichotomous noise, Unimodal-bimodal transition, Non-linear growth models

Posted Date: March 1st, 2021

DOI: https://doi.org/10.21203/rs.3.rs-276324/v1

Noname manuscript No.
(will be inserted by the editor)

Non-Maxwellian distribution in linear systems and its applications

Fernando R. Humire · R. Caicedo · Ernesto Ruppert Filho · M. A. García-Ñustes

Received: date / Accepted: date

Abstract Bimodality is a typical behavior of bistable nonlinear stochastic differential equations. In this work, we find an exact result for calculating the dynamical and stationary probability distribution function in a simple linear system driven by an asymmetric Markovian dichotomous noise. The results show that asymmetric dichotomous noise leads to a unimodal-bimodal distribution transition, exhibiting eight different non-Maxwellian stationary probability distribution profiles in the parameter space. The noise-induced transitions depend on the correlation time, which characterizes the asymmetric dichotomous noise. The calculations are performed using a linear configuration; but applications to other systems governed by nonlinear equations such as single species population growth models are discussed. In the proper limits, the symmetric case, including the Gaussian white noise limit, is recovered. Numerical simulations show good agreement with analytical results. Finally, a possible experimental setup is proposed.

Keywords Non-Maxwellian distribution · Asymmetric dichotomous noise · Unimodal-bimodal transition · Non-linear growth models

Fernando R. Humire (Corresponding author)
Departamento de Física, Facultad de Ciencias, Universidad de Tarapacá, Casilla 7-D Arica, Chile.
E-mail: f.humire@academicos.uta.cl

R. Caicedor · Ernesto Ruppert Filho
Departamento de Sistemas e Energia, Faculdade de Engenharia Elétrica e de Computação, Universidade Estadual de Campinas, Campinas 13083-852, Brasil.

M. A. García-Ñustes
Instituto de Física, Pontificia Universidad Católica de Valparaíso, Casilla 4059, Chile.

1 Introduction

Linear and nonlinear stochastic differential equations have played a crucial and productive role in the theory of out-of-equilibrium phenomena and they have shown that an adequate control of noise can induce interesting phenomena such as stochastic resonance [1,2] and noise-induced transitions [3,4,5]. Several other effects of noise have been studied in [6,7]. Most models are Langevin-type equations, i.e., differential equations of first order with either additive or multiplicative noise terms with respect to the system output. Such noise terms account for fluctuating environment or for controlled noise generated in the laboratory, so statistical properties can be studied.

Usually, in the study of stochastic differential equations (SDE), it is considered a Gaussian white noise, denoted by $\Gamma(t)$. Its correlation function is given by $\langle \Gamma(t)\Gamma(t')\rangle = 2D\delta(t-t')$ where D is the noise strength. However, this is not always realistic. To describe more physical situations, it is necessary to consider a noise with a finite correlation function, e.g., the Ornstein-Uhlenbeck (OU) process or the dichotomous noise. Both processes have a correlation function of decreasing exponential type $\langle \xi(t)\xi(t')\rangle = D/\tau_c \exp(-|t-t'|/\tau_c)$, where τ_c is the correlation time and $\xi(t)$ denotes a colored noise. Unlike the OU process, the dichotomous noise is not Gaussian [8,9]. It belongs to a general family characterized by taking a finite number of random values with a correlation time $\tau_c \neq 0$ [10,11]. In addition, SDEs driven by a dichotomous noise present non-Maxwellian probability distribution, i.e., distributions with a tail that deviates from the Maxwellian one [12]. Non-Maxwellian distributions appear in many areas of science and engineering, for instance, voltage-noise-induced transitions [13], physics of dust-plasma interactions [14],

anomalous velocity distribution [15], the noisy voter model [16], and network models [17].

In general, exact analytical solutions of SDEs for the dynamical and stationary probability distribution are scarce. However, exact solutions have been found in linear stochastic models driven by a symmetric dichotomous noise [15,18]. Symmetric dichotomous noise can also lead, in linear SDEs, transitions from a unimodal to a bimodal symmetric probability distribution [19]. This phenomenon was known to be limited to nonlinear SDEs [3]. Therefore, the kind of noise is relevant to get new phenomena in linear SDEs. However, an asymmetric probability distribution of noise has not been explored yet.

This work study analytically and numerically the transition from a unimodal to a bimodal stationary probability distribution function (PDF) in a linear system driven by an asymmetric dichotomous noise. An exact analytical solution is found for the dynamical and stationary probability distribution as a function of time and the output variable. Noting noise-induced transitions, the study is focused on the stationary PDF, showing that asymmetric dichotomous noise induces eight new solutions. In contrast with symmetric dichotomous noise, which exhibits only two different solutions of the probability distribution. In the proper limits, our results are capable of reproducing the symmetric case including the Gaussian white noise (GWN) case.

Our results can be applied in linear and non-linear systems. For linear systems the analogy is immediate and addresses problems such as neural dynamics [20], the Brownian motion with viscosity [21], and in simple electronic circuits [22,23,24]. In non-linear systems, our results are applied in growth models used to describe the statistical properties of the population dynamics of a single species [25]. Some examples are the growth and decline of the human population in central cities, the spread of epidemics and insects, pollution of the atmosphere, rivers, lakes and seas due to various human activities or also natural disasters. These, and many other phenomena, are typical illustrations of growth phenomena found in many physical and biological areas.

This work is organized in the following way. In section 2, we introduced the linear model driven by an asymmetric dichotomous noise and a constant force. The main statistical properties of asymmetric dichotomous noise and its numerical generation are discussed. In section 3, we calculate analytically the PDF as a function of the output process z and time t. In section 4, transition phenomenon from a unimodal to a bimodal distribution is studied. In the appropriate limits, the symmetric case, including the Gaussian white noise, is recovered. In section 5, applications in growth models are discussed. In particular, we focus our attention on the Gompertz model. The generality of our results is stressed by study some properties of the aforementioned models graphically. In section 6, we check our analytic results numerically and present a possible experimental setup. Finally, conclusions and final remarks are shown in section 7.

2 The stochastic model

Our starting point is defined by a stochastic variable $z(t)$ whose realizations follow a linear Langevin evolution, written as,

$$\frac{d}{dt}z(t) = -\gamma z(t) + V + \sigma\xi_D(t) \tag{1}$$

where $z(t)$ denotes the output variable, γ is the damping parameter, V is a constant average input, and $\xi_D(t)$ is the asymmetric Markovian dichotomous noise with an intensity σ. The dichotomous process $\xi_D(t)$ is also known as random telegraph signal and its state space x consists only of two levels $(a, -b)$. The temporal evolution of the conditional probability $P\left(x,t|\xi_0,t_0\right)$ for the process $\xi_D(t)$ is given by the following master equation [3,26]

$$\begin{pmatrix} \dot{P}\left(a,t|\xi_0,t_0\right) \\ \dot{P}\left(-b,t|\xi_0,t_0\right) \end{pmatrix} = \begin{pmatrix} -\nu_a & \nu_b \\ \nu_a & -\nu_b \end{pmatrix} \begin{pmatrix} P\left(a,t|\xi_0,t_0\right) \\ P\left(-b,t|\xi_0,t_0\right) \end{pmatrix}, \tag{2}$$

where $\xi_0 = \xi_D(t_0)$, ν_a and ν_b are the probabilities by unit time of switching between states $a \to -b$ and $-b \to a$, respectively. In addition, $\tau_j = 1/\nu_j$ are the mean residence time in these states. The conditional probabilities $P\left(a,t|\xi_0,t_0\right)$ and $P\left(-b,t|\xi_0,t_0\right)$ can be obtained by solving the system of equations (2) subject to the initial condition $P\left(x,t|x_0,t_0\right) = \delta_{x,x_0}$, the conservation of total probability $P\left(a,t|\xi_0,t_0\right) + P\left(-b,t|\xi_0,t_0\right) = 1$ and the stationary probabilities

$$P(a,\infty|x,t_0) = P_s(a) = \frac{\nu_b}{\nu_a+\nu_b}, \tag{3a}$$

$$P(-b,\infty|x,t_0) = P_s(b) = \frac{\nu_a}{(\nu_a+\nu_b)}. \tag{3b}$$

where δ_{x,x_0} is the Kronecker delta. These are given by

$$P\left(a,t|\xi_0,t_0\right) = \tau_c\nu_b + \tau_c\left(\nu_a\delta_{a,\xi_0} - \nu_b\delta_{b,\xi_0}\right)\mathrm{e}^{-\frac{(t-t_0)}{\tau_c}} \tag{4a}$$

$$P\left(-b,t|\xi_0,t_0\right) = \tau_c\nu_a - \tau_c\left(\nu_a\delta_{a,\xi_0} - \nu_b\delta_{b,\xi_0}\right)\mathrm{e}^{-\frac{(t-t_0)}{\tau_c}} \tag{4b}$$

with the correlation time $\tau_c = 1/\left(\nu_a+\nu_b\right)$.

The asymmetric dichotomic process is completely determined by Eqs. (4a)-(4b), thus the mean value of

the process $\xi_D(t)$ in the steady state and the correlation function can be calculated as

$$\langle \xi_D(t) \rangle = \sum_{x=-b,a} x P_{st}(x) = \tau_c(\nu_b a - \nu_a b) \quad (5)$$

and

$$\langle \xi_D(t)\xi_D(t') \rangle = \sum_{x,x'} xx' P\left(x,t|x',t'\right) P_{st}(x') = \langle \xi_D(t) \rangle^2 + \frac{\nu_a \nu_b \left(a+b\right)^2}{\left(\nu_a+\nu_b\right)^2} \mathrm{e}^{-\frac{|t-t'|}{\tau_c}}, \quad (6)$$

respectively.

For simplicity, we set the mean value zero $\langle \xi_D(t) \rangle = 0$. Then, $\nu_b = (b/a)\,\nu_a$. If $b/a > 1$, $\nu_b > \nu_a$, on the contrary, if $b/a < 1$, $\nu_b < \nu_a$. Under these conditions, the correlation time becomes $\tau_c = C/\nu_a$ with $C = 1/\left(1+\frac{b}{a}\right)$. If states a and b are fixed, the parameter ν_a controls the correlation time as $\tau_c \sim 1/\nu_a$ (see Fig. 2). In addition, we introduce the parameter Δ_0 that measures the degree of asymmetry of the dichotomous noise, $\Delta_0 \equiv a - b$. The symmetric case is recover by setting $a = b$ and $\nu_b = \nu_a = \nu$. Accordingly, the asymmetric dichotomous Markov process is characterized by three independent parameters a, b and ν_a.

The dichotomic noise converges to Gaussian white noise through an appropriate limit procedure [8,9]. Applications and experimental evidence can been found in the literature [3,27,28].

2.1 Statistical properties of the output process $z(t)$

Formally integrating the Eq. (1) and setting the initial condition $z(t_0 = 0) = z_0$, we get

$$z(t) = z_0 \mathrm{e}^{-\gamma t} + \int_0^t ds(\sigma\xi(s) + V)\mathrm{e}^{-\gamma(t-s)}. \quad (7)$$

From this equation and using the statistical properties of process $\xi_D(t)$ in (5)-(6), it is possible to calculate the mean value and correlation function of the output stochastic process $z(t)$. First, we take the mean value over all realizations of the process $\xi_D(t)$ on the Eq. (7). Then, we have in the steady state ($t \to \infty$),

$$\langle z(t) \rangle_s = \frac{V}{\gamma}. \quad (8)$$

Next, putting for simplicity $z_0 = 0$ and considering (5), the correlation function is given by

$$\langle z(t)z(t') \rangle = \left(\frac{V}{\gamma}\right)^2 \left(1-\mathrm{e}^{-\gamma t}\right)\left(1-\mathrm{e}^{-\gamma t'}\right) + \sigma^2 \int_0^t ds \int_0^{t'} ds' \mathrm{e}^{-\gamma(t-s)} \mathrm{e}^{-\gamma\left(t'-s'\right)} \langle \xi_D(s)\xi_D(s') \rangle, \quad (9)$$

using property (6) and centering on the stationary state $t \to \infty$ and $t' \to \infty$ with $|t-t'|$ finite, we obtain

$$\langle z(t)z(t') \rangle = \left(\frac{V}{\gamma}\right)^2 - \frac{ab\sigma^2\mu_c}{\gamma\left(\gamma^2-\mu_c^2\right)} \mathrm{e}^{-\gamma|t-t'|} + \frac{ab\sigma^2}{\left(\gamma^2-\mu_c^2\right)} \mathrm{e}^{-\mu_c|t-t'|}. \quad (10)$$

here $\mu_c = 1/\tau_c$. The realizations of the variable $z(t)$ can be found by numerically integrating Eq. (1). We used the Euler-Maruyama scheme with a time step $\Delta t = 0.01(s)$. Fig. 1 shows $z(t)$ for three values of the $\nu_a = 6, 80$ and 100 with their corresponding stationary histograms (see right panel). The Figs. 1(a) and 1(b) show the asymmetric case with parameters $a = 3$ and $b = 1$. In Fig.1(a), it is shown that the realization $z(t)$ has a bimodal stationary PDF, while in Fig.1(b) has a unimodal distribution. These latter are known as non-Maxwellian distribution [12,15,22]. Figure 1(c) shows numerically the transition from non-Maxwellian to Maxwellian distribution in the limit to GWN with parameters $\nu_a = 100$ and $a = b = 5$. Returning to Figs. 1(a)-(b), it is observed that a transition from a bimodal to a unimodal stationary PDF occurs. This transition is controlled by the parameter that characterizes noise ν_a. In the following sections, analytical and numerical analysis of the phenomenon of transition from a unimodal

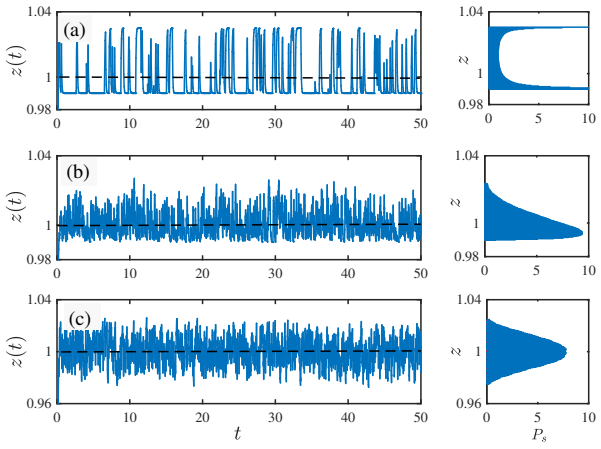

Fig. 1: (Color online) Realizations of the output process $z(t)$ with their corresponding histograms (right panels). The black dashed line is the mean value $\langle z(t) \rangle_s = 1$. a) An asymmetric bimodal distribution with parameters $a = 3$, $b = 1$, and $\nu_a = 6$. b) An asymmetric unimodal distribution with parameters $a = 3$, $b = 1$, and $\nu_a = 80$. c) The symmetric case with parameters $a = b = 5$ and $\nu_a = 100$.

to a bimodal non-Maxwellian stationary distribution is shown.

2.2 Generation of asymmetry dichotomous noise

This subsection is devoted to the generation of asymmetric dichotomous noise. This noise is a random stationary Markovian process that consists of jumps between two states a and $-b$. The jumps follow in time a Poisson process and the conditional probabilities between the two states can be obtained from (4a)-(4b) as follows

$$P_{aa} = \tau_c \left(\nu_b + \nu_b \mathrm{e}^{-(t-t_0)/\tau_c}\right), \tag{11a}$$

$$P_{ab} = \tau_c \nu_b \left(1 - \mathrm{e}^{-(t-t_0)/\tau_c}\right), \tag{11b}$$

$$P_{bb} = \tau_c \left(\nu_a + \nu_b \mathrm{e}^{-(t-t_0)/\tau_c}\right), \tag{11c}$$

$$P_{ba} = \tau_c \nu_b \left(1 - \mathrm{e}^{-(t-t_0)/\tau_c}\right). \tag{11d}$$

We follow the numerical algorithm for the dichotomous sequence $\xi_D(t)$ introduced in Refs. [29,30]. Figures 2(a) and 2(b) show two realizations of the asymmetric case considering the values of $a = 3$ and $b = 1$. In Fig. 2(a) the inverse of the correlation time is given by $\nu_a = 1$ ($\nu_b = (b/a)\,\nu_a = 1/3$) and its respective mean residence time is $\tau_a = 1/\nu_a = 1$ ($\tau_b = 1/\nu_b = 3$). In Fig. 2(b) the inverse of the correlation time is given by $\nu_a = 6$ ($\nu_b = (b/a)\,\nu_a = 2$) and its respective mean residence time is $\tau_a = 1/\nu_a = 1/6$ ($\tau_b = 1/\nu_b = 1/2$). Comparing figures 2(a) and 2(b), we can clearly observe that the mean residence time in each state decreases from $\tau_a = 1$ to $\tau_a = 1/6$ and from $\tau_b = 3$ to $\tau_b = 1/2$ when the inverse of the correlation time ν_a ($\sim 1/\tau_c$) increases. In other words, noise is increasingly uncorrelated, in agreement with the theory (Eqs. (4)-(6)). The Fig. 2(c) shows a realization of the symmetric case considering the values $a = b = 1$ and $\nu_a = \nu_b = \nu = 1$. The degree of asymmetry is given by the parameter $\Delta_0 = 2$ and $\Delta_0 = 0$, respectively.

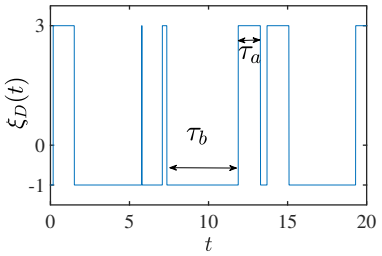

(a) The asymmetric case considering the values $a = 3$, $b = 1$, $\nu_a = 1$, and $\nu_b = 1/3$.

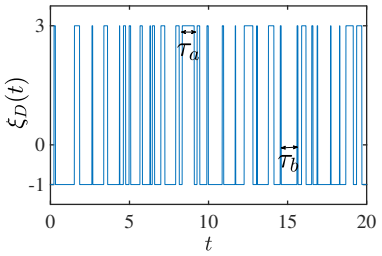

(b) The asymmetric case considering the values $a = 3$, $b = 1$, $\nu_a = 6$, and $\nu_b = 2$.

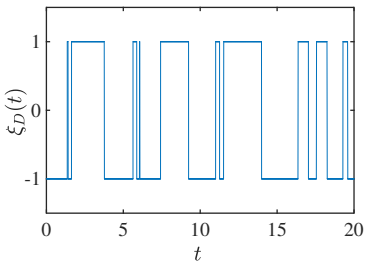

(c) The symmetric case considering the values $a = b = 1$ and $\nu_a = \nu_b = \nu = 1$.

Fig. 2: (Color online) Realizations of the dichotomous noise $\xi_D(t)$ as a function of time t.

3 The exact probability distribution

In this section, it is obtained analytically the probability distribution function $P(z,t)$ of the process $z(t)$ defined by Eq. (1). Starting with the displacement $z(t) = y(t) + V/\gamma$ in the Eq. (1) such as,

$$\dot{y}(t) = -\gamma y + \sigma \xi_D(t). \tag{12}$$

The stochastic Liouville equation for the density function $\rho(y,t;\xi_D)$ of Eq. (12) [31] is

$$\frac{\partial}{\partial t}\rho(y,t;\xi_D) = \gamma\rho(y,t;\xi_D) + \gamma y \frac{\partial}{\partial y}\rho(y,t;\xi_D) - \sigma \frac{\partial}{\partial y}\xi_D(t)\rho(y,t;\xi_D), \tag{13}$$

taking the mean value over all the realizations of process $\xi_D(t)$ and using the Van Kampen's lemma, the following expression is obtained,

$$\frac{\partial P}{\partial t} = \gamma P + \gamma y \frac{\partial P}{\partial y} - \sigma \frac{\partial P_1}{\partial y}, \tag{14}$$

where $P \equiv P(y,t) \equiv \langle \rho(y,t;\xi_D) \rangle$ and $P_1 \equiv P_1(y,t) = \langle \xi_D(t)\rho(y,t;\xi_D) \rangle$. Now, using the well-know Shapiro-

Loginov formula for differentiation of exponentially correlated stochastic functions [32], the partial differential equation for the function $P_1(y,t)$ takes the form,

$$\frac{\partial P_1}{\partial t} = (\gamma - N)\, P_1 + \gamma y \frac{\partial P_1}{\partial y} - \sigma \frac{\partial}{\partial y} \left\langle \xi_D^2(t) \rho(y,t;\xi_D) \right\rangle \tag{15}$$

where $N = \nu_a + \nu_b$. Using the property of dichotomous noise $\xi_D^2(t) = \Delta^2 + \Delta_0 \xi_D(t)$, where $\Delta^2 = ab$ and $\Delta_0 = a - b$ [9], Eq. (15) is transformed in

$$\frac{\partial P_1}{\partial t} = (\gamma - N) P_1 + (\gamma y - \sigma \Delta_0) \frac{\partial P_1}{\partial y} - \sigma \Delta^2 \frac{\partial P}{\partial y}. \tag{16}$$

The system of Eqs. (14) and (16) allows us to find an exact equation for the probability distribution $P(z,t)$ of the stochastic model (1). In general, it is difficult to obtain a closed equation for $P(z,t)$. Differentiating with respect to time Eq. (14)

$$\frac{\partial^2 P}{\partial t^2} = \gamma \frac{\partial P}{\partial t} + \gamma y \frac{\partial P}{\partial y \partial t} - \sigma \frac{\partial P_1}{\partial y \partial t}. \tag{17}$$

and taking the derivative with respect to y on Eq. (16), we get

$$\frac{\partial P_1}{\partial y \partial t} = (2\gamma - N) \frac{\partial P_1}{\partial y} + (\gamma y - \sigma \Delta_0) \frac{\partial^2 P_1}{\partial y^2} - \sigma \Delta^2 \frac{\partial^2 P}{\partial y^2}. \tag{18}$$

Combining equations (17) and (18), we finally obtain the equation of evolution for $P(z,t)$

$$\frac{\partial^2 P}{\partial t^2} - 2\gamma \left(y - \frac{\sigma \Delta_0}{2\gamma} \right) \frac{\partial^2 P}{\partial y \partial t} + \gamma^2 \left[\left(y - \frac{\sigma \Delta_0}{2\gamma} \right)^2 - \left(\frac{\sigma \Delta}{\gamma} \right)^2 - \left(\frac{\sigma \Delta_0}{2\gamma} \right)^2 \right] \frac{\partial^2 P}{\partial y^2} - (3\gamma - N) \frac{\partial P}{\partial t} + \gamma \left[(4\gamma - N) y - 2\sigma \Delta_0 \right] \frac{\partial P}{\partial y} + (2\gamma - N) \gamma P = 0. \tag{19}$$

Additionally, two initial conditions are required for the evolution of Eq. (19). The first initial condition is given by $P(y,0) = \delta(y)$, whereas the second initial condition can be obtained from a hypothesis of the Shapiro-Loginov formula, which indicates the statistical independence between $\xi_D(t)$ and $\rho(y,t;\xi_D)$ at the initial time $t = 0$. Therefore, $\langle \xi_D(t) \rho(y,t;\xi_D) \rangle \,|_{t=0} = 0$. Consequently the initial conditions are

$$P(y,t)\,|_{t=0} = \delta(y), \left(\frac{\partial}{\partial t} - \gamma y \frac{\partial}{\partial y} - \gamma \right) P(y,t)\,|_{t=0} = 0. \tag{20}$$

The following change of variables,

$$y = x + \kappa, \qquad t = \frac{\tau}{\gamma}, \tag{21}$$

with $\kappa = \Delta_0\ \sigma/2\gamma$, further simplifies Eq. (19) and remembering the relations for Δ and Δ_0 then the equation for the probability density can be written as

$$\frac{\partial^2 P}{\partial \tau^2} - 2x \frac{\partial^2 P}{\partial \tau \partial x} + \left(x^2 - \lambda^2 \right) \frac{\partial^2 P}{\partial x^2} - (1 + \mu) \frac{\partial P}{\partial \tau} + \left((2 + \mu) x - (2 - \mu) \kappa \right) \frac{\partial P}{\partial x} + \mu P = 0 \tag{22}$$

here $\lambda = \sigma (a + b)/2\gamma$, $\mu = 2 - N/\gamma$, and their initial conditions are given by

$$P(x,\tau)\,|_{\tau=0} = \delta(x + \kappa), \tag{23a}$$

$$\left(\frac{\partial}{\partial \tau} - (x + \kappa) \frac{\partial}{\partial x} - 1 \right) P(x,\tau)\,|_{\tau=0} = 0,$$

$$\frac{\partial P}{\partial \tau}|_{\tau=0} = (x + \kappa)\, \delta'(x + \kappa) + \delta(x + \kappa). \tag{23b}$$

This is a Cauchy problem. The standard approach to find the solution of system (22)-(23), begins with its reduction to the canonical form. First, we introduce the following in Eq. (22)

$$P(x,\tau) = U(x,\tau)\, \mathrm{e}^{\mu \tau}, \tag{24}$$

such as

$$\frac{\partial^2 U}{\partial \tau^2} - 2x \frac{\partial^2 U}{\partial x \partial \tau} + \left(x^2 - \lambda^2 \right) \frac{\partial^2 U}{\partial x^2} + (\mu - 1) \frac{\partial U}{\partial \tau} - (\mu - 2)(x - \kappa) \frac{\partial U}{\partial x} = 0. \tag{25}$$

Transforming Eq. (25) by using the new variables ϕ and θ, defined by the following nonlinear transformation

$$x = \lambda \frac{\theta + \phi}{\theta - \phi}, \qquad \tau = \ln \left(\frac{1}{2\lambda} (\theta - \phi) \right), \tag{26}$$

we get

$$\frac{\partial^2 U}{\partial \phi \partial \theta} + \frac{1}{(\theta - \phi)} \left[\alpha_2 \frac{\partial U}{\partial \phi} - \alpha_1 \frac{\partial U}{\partial \theta} \right] = 0 \tag{27}$$

where

$$\alpha_1 = 1 - \frac{Na}{\gamma (a + b)}, \quad \alpha_2 = 1 - \frac{Nb}{\gamma (a + b)}. \tag{28}$$

This equation is the Euler-Darboux equation and its solution is widely studied in Refs. [33,34]. The final step is to solve the Cauchy problem associated with Eq. (27) and initial conditions Eq. (23). For this, we

used the Riemann method described in the Ref. [33]. We thus find the following solution

$$P(x,\tau) = \frac{1}{2}\mathrm{e}^{(\alpha_1-1)\tau}\delta\left(x-\Lambda_a^-\right) + \frac{1}{2}\mathrm{e}^{(\alpha_2-1)\tau}\delta\left(x+\Lambda_b^-\right) + Q(x,\tau)\,{}_2F_1\left[\alpha_1,\alpha_2;1;\epsilon\right] + W(x,\tau)\,{}_2F_1\left[\beta_1,\beta_2;2;\epsilon\right] \quad (29)$$

here $\Lambda_a^{\pm} = \lambda \pm (a\sigma/\gamma)\mathrm{e}^{-\tau}$, $\Lambda_b^{\pm} = \lambda \pm (b\sigma/\gamma)\mathrm{e}^{-\tau}$, $\delta(\cdot)$ is the Dirac delta function, ${}_2F_1\left[\cdot;\epsilon\right]$ is the Gauss hypergeometric function, with

$$Q = \frac{(1-\mu)}{(2\lambda)^{1-\mu}}\left(\Lambda_b^+ - x\right)^{-\alpha_1}\left(\Lambda_a^+ + x\right)^{-\alpha_2} \times \left[1 + \frac{\sigma/\gamma\mathrm{e}^{-\tau}}{(1-\mu)}\left(a\alpha_1\left(\Lambda_b^+ - x\right) + b\alpha_2\left(\Lambda_a^+ + x\right)\right)\right], \quad (30a)$$

$$W = \alpha_1\alpha_2\mathrm{e}^{-\tau}(2\lambda)^{\mu+1}\left(\Lambda_b^+ - x\right)^{-(\beta_1+1)}\left(\Lambda_a^+ + x\right)^{-(\beta_2+1)} \times \left[-x^2 - 4\kappa\mathrm{e}^{-\tau}x + (\Lambda_a^+\Lambda_a^- + \Lambda_b^+\Lambda_b^-)/2 - 2\kappa^2\mathrm{e}^{-2\tau}\right], \quad (30b)$$

where $\beta_{1,2} = \alpha_{1,2} + 1$, and

$$\epsilon = \frac{\left(x-\Lambda_a^-\right)\left(x+\Lambda_b^-\right)}{\left(x+\Lambda_a^+\right)\left(x-\Lambda_b^+\right)}. \quad (31)$$

The solution (29) has a domain given by $-\Lambda_a^+ \le x \le \Lambda_b^+$, otherwise the probability density is zero $P(x,\tau) = 0$. Finally, with the help of Eq. (21) we can write the probability density (29) as a function of the original variables (z,t), as

$$P(z,t) = P\left[x \to z - \frac{V}{\gamma} - \kappa, \gamma t\right] \quad (32)$$
$$-\lambda - (a\sigma/\gamma)\mathrm{e}^{-\gamma t} \le z - V/\gamma - \kappa \le \lambda + (b\sigma/\gamma)\mathrm{e}^{-\gamma t}.$$

4 The stationary distribution

From now on, we focus on the stationary probability distribution function $P_s(z)$ and its properties, in particular, we characterize the transition from a unimodal to a bimodal distribution. Taking the limit $t \to \infty$ in Eq. (32), the terms proportional to the expression $\mathrm{e}^{-\tau}$ go to zero, i.e., $\Lambda_a^{\pm} \to \lambda$, $\Lambda_b^{\pm} \to \lambda$, $W(x,\tau) \to 0$, $\epsilon \to 1$. Thus, Dirac delta functions can be neglected, being the dominant term $Q(x,\tau)$. This leads to the stationary PDF $P_s(z)$. Conversely, when $t \to 0$, the dominant terms in (32) are Dirac delta functions travelling in opposite directions, which is characteristic of a dichotomous process $\xi_D(t)$. The transient effects of $P(z,t)$ will not be discussed here.

Next, we take the limit $t \to \infty$ and obtain

$$P_s(z) = \frac{(1-\mu)}{(2\lambda)^{1-\mu}}\left(\frac{a\sigma}{\gamma} + \left(\frac{V}{\gamma} - z\right)\right)^{-\alpha_1} \times \left(\frac{b\sigma}{\gamma} - \left(\frac{V}{\gamma} - z\right)\right)^{-\alpha_2} F\left[\alpha_1,\alpha_2;1;\epsilon\to 1\right] \quad (33)$$

The argument of the hypergeometric function ϵ tends to one in the stationary state. We use Gauss' theorem [35] to rewrite expression (33) in the following form

$$P_s(z) = \frac{(1-\mu)}{(2\lambda)^{1-\mu}}\frac{\Gamma(1-\mu)}{\Gamma(1-\alpha_1)\Gamma(1-\alpha_2)} \times \left(\frac{\sigma a}{\gamma} + \left(\frac{V}{\gamma} - z\right)\right)^{-\alpha_1}\left(\frac{\sigma b}{\gamma} - \left(\frac{V}{\gamma} - z\right)\right)^{-\alpha_2} \quad (34)$$

here $\Gamma(\cdot)$ is the Gamma function, P_s has a domain given by $(V-\sigma b)/\gamma \le z \le (V+\sigma a)/\gamma$. The probability distribution is zero, $P_s(z) = 0$, otherwise.

First, we studied the symmetric case $a = b$ and $\nu_a = \nu_b = \nu$, thus, it is seen that Eq. (34) may be written as

$$P_s(z) = \frac{(1-\mu)}{(2\lambda)^{1-\mu}}\frac{\Gamma(1-\mu)}{\Gamma^2(1-\alpha)}\left(\left(\frac{\sigma a}{\gamma}\right)^2 - \left(\frac{V}{\gamma} - z\right)^2\right)^{-\alpha} \quad (35)$$

where $\alpha = (1-\nu/\gamma)$ and $(V-\sigma a)/\gamma \le z \le (V+\sigma a)/\gamma$. Expression (35) describes the transition from a unimodal to a bimodal distribution, which is controlled by the inverse of the correlation time of the symmetric dichotomous noise ν. The transition occurs when $\alpha = 0$, at $\nu^c = \gamma$. If $\nu < \nu^c$ ($\alpha > 0$) the Eq. (35) has a minimum in the mean value $\langle z(t)\rangle = V/\gamma$ and its tails go to infinity (bimodal distribution). While if $\nu > \nu^c$ ($\alpha < 0$) the Eq. (35) has a maximum in $\langle z(t)\rangle = V/\gamma$ and its extremes go to zero (unimodal distribution).

Figure (3) displays the stationary probability distribution in the symmetric case as a function of the z process with $\gamma = 0.5$, $V = 1.5$, and $\sigma = 0.5$. We used five different values of the inverse of the correlation time ν, namely, $\nu = 0.1, 0.3, 0.5, 1.0$ and 10. The transition from a bimodal to a unimodal distribution occur in $\nu^c = \gamma = 0.5$. For the values of $\nu = 0.1$ and 0.3 the distribution has a minimum since $\nu < \nu^c$, while for the values $\nu = 0.5$ and 1.0, it has a maximum since $\nu > \nu^c$. Taking appropriate limits on the parameters $\nu \to \infty$, $a \to \infty$ and keeping the ratio finite $r = a^2/\nu$, the current distribution (35) goes asymptotically to the Maxwellian distribution $P_s(z) = 1/(\sqrt{2\pi}D)\mathrm{e}^{-(z-V/\gamma)^2/2D^2}$. This limit corresponds to the Gaussian white noise, where the expression $D^2 = \sigma^2 r/(2\gamma)$ must remain constant [21]. The Fig. (3), with $\nu = 10$ (yellow marker line), shows the probability distribution in the numerical limit to the GWN.

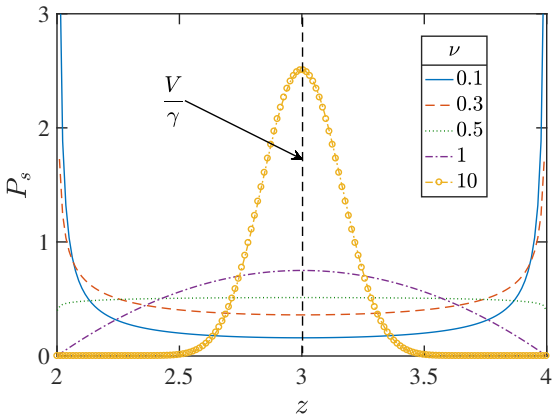

Fig. 3: (Color online) The symmetric stationary probability distribution $P_s(z)$ as a function of z with parameter values $a = b = 1$ and $\nu_a = \nu_b = \nu = 0.1$ (blue solid line), 0.3 (orange dashed line), 0.5 (green dotted line), 1.0 (purple dash-dot line). When $\nu = 10$ (yellow marker line), we recover the limit to GWN. The other parameters values are $\gamma = 0.5$, $V = 1.5$, and $\sigma = 0.5$

Next, we study the effects produced by an asymmetric dichotomous noise on model (1), for this, we return to Eq. (34). In this case, the transitions are controlled by the parameters α_1 and α_2, where $\alpha_1 \neq \alpha_2$. Using the equation $\nu_b = (b/a)\,\nu_a$ (zero mean condition) and Eq. (28), we can rewrite α_1 and α_2 as a function of ν_a in the following form

$$\alpha_1(\nu_a) = 1 - \nu_a/\gamma, \tag{36a}$$
$$\alpha_2(\nu_a) = 1 - (b/a)\,\nu_a/\gamma. \tag{36b}$$

Figure 4(a) shows parameters (36) as a function of ν_a for $\Delta_0 = a - b > 0$. Three regions R:(I)-(III) are separated by vertical dashed lines. The transition from a bimodal to a unimodal distribution occurs when $\alpha_1 = 0$ at the transition point $\nu_a^c = \gamma = 0.5$, exactly in the border of regions R:(I)→(II). For values in the range $\nu_a^c < \nu_a < (a/b)\gamma = 1.5$, the parameter $\alpha_1 < 0$ and $\alpha_2 > 0$, such the left tail of $P_s(z)$ remains infinite (see Fig. 4(b) with $\nu_a = 0.5$). When $\alpha_2 = 0$ at the point $\nu_a = (a/b)\gamma = 1.5$, exactly in the border of region R:(II)→(III), the left tail becomes zero.

Figure 4(b) shows the behavior of $P_s(z)$ in each region of the Fig. 4(a) for four different values of the inverse of the correlation time ν_a, namely, $\nu_a = 0.1, 0.5, 1.0$ and 2.0. We have a bimodal distribution for $\nu_a = 0.1$ (R:(I)). For $\nu_a = 0.5$ (R:(II)), a unimodal distribution with infinite tail appears. Finally, for $\nu_a = 1.0$ and 2.0 (R:(III)), we observe a unimodal distribution with finite tails. In this context, we can observe that when $\Delta_0 > 0$, the distribution $P_s(z)$ is asymmetric with respect to the mean value $\langle z(t)\rangle = V/\gamma = 3$. For values of $\nu_a > \nu_a^c$, the maximum of the probability is on the left side of the mean value. Table (1) summarizes the behavior of $P_s(z)$ for different combinations of α_1 and α_2.

Figure 5(a) shows parameters α_1 and α_2 as a function of ν_a with the parameter of asymmetry negative $\Delta_0 = a - b < 0$. In this case, the slope of α_2 is $b/a > 1$, allowing that the transition from region R:(I)→(II) be controlled by the parameter α_2 and not by the parameter α_1 as in Fig. 4. Then for $\Delta_0 < 0$, the transition point is $\nu_a^c = (a/b)\gamma = 1/6$ ($\alpha_2 = 0$). For $\nu_a^c < \nu_a < \gamma = 0.5$, $\alpha_1 > 0$ and $\alpha_2 < 0$, the right tail of $P_s(z)$ remains infinite (see Fig. 5(b) with $\nu_a = 0.5$). When $\alpha_1 = 0$ at the point $\nu_a = \gamma$ (border R:(II)→(III)), the right tail becomes zero.

Figure 5(b) shows the behavior of $P_s(z)$ for four values of ν_a, namely, $\nu_a = 0.1, 0.2, 1.0$ and 2.0. We observe a bimodal distribution at $\nu_a = 0.1$ (R:(I)). For $\nu_a = 0.2$ (R:(II)) and $\nu_a = 1.0, 2.0$ (R:(III)), we obtain a unimodal distributions with infinite and finite tails, respectively. Table (2) summarizes the behavior of $P_s(z)$ for different combinations of α_1 and α_2.

The phase diagram of the stochastic model (1) in terms of the variables Δ_0 and ν_a is displayed in Fig. 6. The plot was separated into six regions, the regions R:(I)-(III) for $\Delta_0 > 0$, the regions R:(IV)-(VI) for $\Delta_0 < 0$ and the symmetric case over the line $\Delta_0 = 0$. For increasing ν_a, a bimodal to a unimodal transition occurs *i) at* $\nu_a^c = \gamma$ ($\alpha_1 = 0$) *for* $\Delta_0 > 0$ and *ii)* for $\Delta_0 < 0$, over the line given by $\Delta_0^c = -(a\gamma)/\nu_a + a$ ($\alpha_2 = 0$). Conversely, an infinite to finite tail transition occurs, *i)* for $\Delta_0 > 0$, on the green dashed line $\Delta_0 = (b/\gamma)\nu_a - b$ ($\alpha_2 = 0$) and *ii)* for $\Delta_0 < 0$, at the point $\nu_a = \gamma$ ($\alpha_1 = 0$).

5 Application

In this section, we apply the analytical results reported in Section 4 in linear and nonlinear systems. At first, the results can be applied directly in first-order linear systems as a series RL circuit. But, more interestingly, the results can also be adapted to non-linear systems by a non-linear change of variable. In the latter, we obtain the stationary probability distribution and study the different transitions graphically.

5.1 The resistive-inductive circuit model

The stochastic model (1) can be found in many physical and engineering systems. In Refs. [22,23], the authors

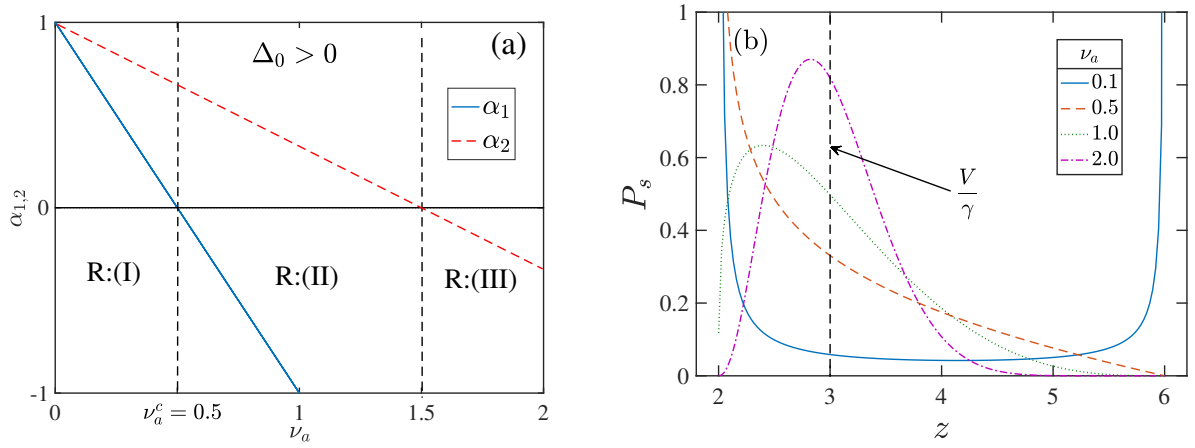

Fig. 4: (Color online) (a) Parameters α_1 and α_2 as a function of the inverse of the correlation time ν_a. (b) The asymmetric stationary probability distribution $P_s(z)$ for several values of the inverse of the correlation time, $\nu_a = 0.1$ (blue solid line), 0.5 (orange dashed line), 1.0 (green dotted line) and 2.0 (purple dash-dot line). The other parameters values are $a = 3$, $b = 1$, $\gamma = 0.5$, $V = 1.5$, and $\sigma = 0.5$.

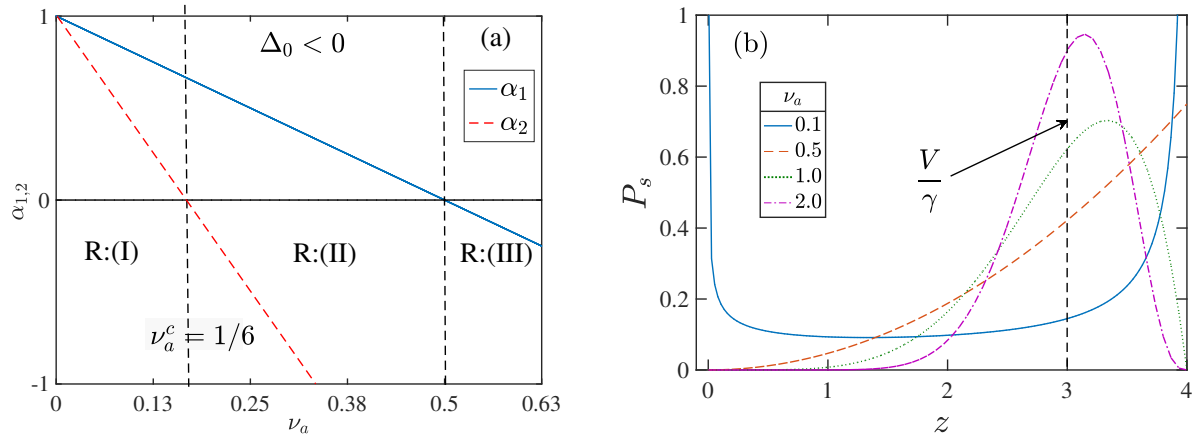

Fig. 5: (Color online) (a) Parameters α_1 and α_2 as a function of ν_a. (b) The asymmetric stationary probability distribution $P_s(z)$ for several values of $\nu_a = 0.1$ (blue solid line), 0.5 (orange dashed line), 1.0 (green dotted line) and 2.0 (purple dash-dot line). The other parameters values are $a = 1$, $b = 3$, $\gamma = 0.5$, $V = 1.5$, and $\sigma = 0.5$

Table 1: Different behaviors of $P_s(z)$ for $\Delta_0 > 0$.

	R:(I)	R:(II)	R:(III)
Sign of α	$\alpha_1, \alpha_2 > 0$	$\alpha_1 < 0, \alpha_2 > 0$	$\alpha_1, \alpha_2 < 0$
Distribution type	bimodal/infinite tails	unimodal/left tail infinite	unimodal/finite tails

Table 2: Different behaviors of $P_s(z)$ for $\Delta_0 < 0$.

	R:(I)	R:(II)	R:(III)
Sign of α	$\alpha_1, \alpha_2 > 0$	$\alpha_1 > 0, \alpha_2 < 0$	$\alpha_1, \alpha_2 < 0$
Distribution type	bimodal/infinite tails	unimodal/left tail infinite	unimodal/finite tails

used GWN on an RC filter whose output is limited and applied on a second RC filter. They found an iterative

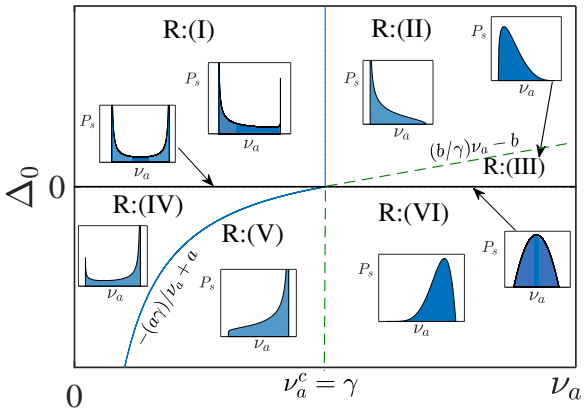

Fig. 6: (Color online) Phase diagram of the model (1) as a function of the asymmetry parameter Δ_0 and the inverse of the correlation time ν_a. The blue solid line and green dashed line separate six regions R:(I)-(VI). Regions R:(I)-(III) correspond to $\Delta_0 > 0$ and for $\Delta_0 < 0$ we have regions R:(IV)-(VI). Inset: different behaviors of the stationary probability distribution.

scheme to determine the moments of the system and obtain information about the behavior of the probability distribution. The model (1) can also represent the evolution of a Brownian particle subject to dichotomic force or other statistical forces as a model of neural dynamics called the leaky integrate-and-fire model [20], the evolution equation for a resistive-capacitive circuit [24] or an RLC circuit in the overdamped limit driven by a fluctuating source [26].

Here, our starting point is the resistive-inductive stochastic electrical circuit

$$L\dot{I}(t) = -RI(t) + V + V_0\xi_D(t) \tag{37}$$

where $I(t)$ denotes the electric current intensity, R is the resistance, L is the inductance, V is the DC input voltage, and $\xi_D(t)$ is the asymmetric Markovian dichotomous noise with an intensity V_0.

Equation (37) is directly transformed into the initial model (1) considering the changes $\gamma = R/L$ and $\sigma = V_0/L$. Thus, the series RL circuit driven by an asymmetric dichotomous noise has access to eight different behaviors of the probability distribution (see Fig. (6)).

5.2 The nonlinear model

The results can be applied to a set of nonlinear equations that are reducible to linear equations through a nonlinear transformation. In particular, the Gompertz model [25] proposed to describe human adult mortality tables have a wide range of applicability in growth population studies as tumors cells in a confined space [36,37,38] . The model is given by

$$\dot{u} = -ru\ln\left(\frac{u}{N}\right) \tag{38}$$

where r is the deterministic growth rate and N is the carrying capacity.

Modifying the parameter N in the form $\ln(N) \longrightarrow \ln(N_0) + a_1\xi_D(t)$, being $\xi_D(t)$ the Markovian asymmetric dichotomic noise studied in Section 2, N_0 the mean value of the carrying capacity, and a_1 a constant that measures the intensity of the stochastic fluctuations about the mean value, we obtain the following ordinary SDE

$$\dot{u} = -ru\ln\left[\frac{u}{N(N_0,\xi_D(t))}\right]. \tag{39}$$

Using the Stratonovich interpretation of the stochastic differential equation, we can perform the following change of variable

$$z(t) = \frac{1}{r}\ln\left(\frac{u(t)}{N_0}\right), \tag{40}$$

which formally maps Eq. (39) in Eq. (1)

$$\dot{z} = -rz + a_1\xi_D(t). \tag{41}$$

with $\gamma = r$, $\sigma = a_1$, and $V = 0$. Then the probability distribution function for the Gompertz model is

$$P_s(u) = \frac{1}{ru}p\left[z \to \frac{1}{r}\ln\left(\frac{u}{N_0}\right)\right] \tag{42}$$

where $p(z)$ is given by Eq. (34). The presence of noise in growth models can be justified in a real situation. In general, this is because the environmental factors that influence population growth are not deterministic, some of these factors may be the number of resources, birth and death rates, and the balance between immigration and emigration rates. Hence, random fluctuations in growth models have been considered in many places in the literature [3,25,31,37]. Figure 7 shows the stationary probability distribution as a function of u for two values of the parameter $\nu_a = 0.5$ and 1.5. For $\nu_a = 0.5$, we observe that $P_s(u)$ has two maxima whereas for $\nu_a = 1.5$ the distribution has only one maximum, that is, the probability distribution function undergoes a noise-induced transition. We can also observe an asymmetric form of the distribution function which is inherited from the asymmetry property of dichotomous noise.

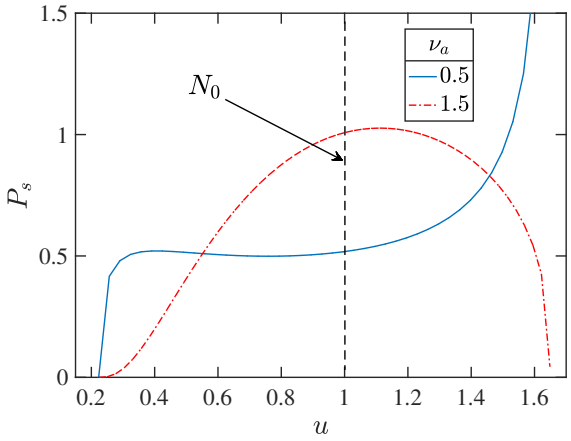

Fig. 7: (Color online) The asymmetric stationary probability distribution $P_s(u)$ for two values of $\nu_a = 0.5$ (blue solid line) and 1.5 (red dashed line). Parameter values are $a = 1$, $b = 3$, $a_1 = 0.5$, $N_0 = 1$, and $r = 1.1$.

Finally, we can consider the following nonlinear stochastic differential equation

$$\frac{du}{dt} = g(u) + ah(u)\xi_D(t) \tag{43}$$

such that the functions $g(u)$ and $h(u)$ fulfill the relation

$$h(u)\frac{dg}{du} = -kh(u) + g(u)\frac{dh}{du} \tag{44}$$

here k depends on parameters of the system under study, for example, for Gomperzt model (39) $k = rN_0$. Then, using the change of variable $dz = du/h(u)$ the previous equation (43) is reduced to a linear stochastic equation

$$\frac{dz}{dt} = -rz + a\xi_D(t) \tag{45}$$

Hence, in terms of the original variable u, the corresponding stationary probability distribution function is given by

$$P_s(u) = P_s\left[z(u)\right]\frac{dz}{du}. \tag{46}$$

Another model that can be reduced using a change of variable is the Hongler model. This model has not found physical applications, however, it can be approximated to the genetic model which is widely used in genetics and chemistry [3].

6 Numerical check and possible experimental setup

Let us focus on a resistive-inductive circuit (RL circuit) due to its simplicity and considerable interest from the fundamental and applied point of view. Passive simple electronic circuits are truly linear and flexible systems to promote our theoretical predictions and they provide real and close motivation for future implementation. RL circuits can be found at the basic elements of a large number of useful devices such as DC-DC converter [39], CMOS logic gate [40,41], electronic filters [42], electric transmission lines [29], among others. Therefore, a deeper understanding of an RL stochastic model could be relevant for the control of instabilities in complex devices.

To validate the analytical results, we numerically integrate Eq. (37) using the Euler-Maruyama method with a time step $\Delta t = 0.001(s)$ and parameter values given by $R = 1(\Omega)$, $L = 0.05(H)$, $V = 1.0(V)$, and $V_0 = 0.01(V)$. The theoretical and numerical stationary probability distributions are shown in Fig. 8. Figure 8(a) and 8(b) show the symmetric and asymmetric case, respectively. Numerical results are in good agreement with the theory.

Next, we propose a possible experimental setup to take into account the influence of the asymmetric dichotomous noise on the R-L circuit. There are standard methods available to generate the dichotomous signal discussed here. For example, a bistable multivibrator with symmetric output activated with a Geiger-Muller [24] or through the use of an acoustic-optic modulator coupled to a signal generator [28].

The experimental proposal is shown in Fig. 9(a). It consists of a constant potential source in series with a linear resistance R and an inductor L. Such combination is connected in series with a source of dichotomic alternating voltage. The dichotomic source consists of a selector switch, $S(t)$, of two levels connected to two sources with different voltage levels (High/Low) (see Fig. 9(b)). The $S(t)$ switch must be controlled according to the Poisson statics.

Some important technical problems can surge in the physical implementation of the experiment, firstly, the switch non-ideal behavior must be taken into account. Secondly, arc effects can occur when the switch is opening or closing. These effects can induce an additional source of noise, leading to a misinterpretation of the experimental results. This uncontrolled source of noise can be considered in the theory as a Gaussian white noise $\Gamma(t)$. Thus, the new voltage input could be of the form $V_{input} = a_1\xi_D(t) + a_2\Gamma(t)$. A complete analysis of the possible configuration for this experiment will be

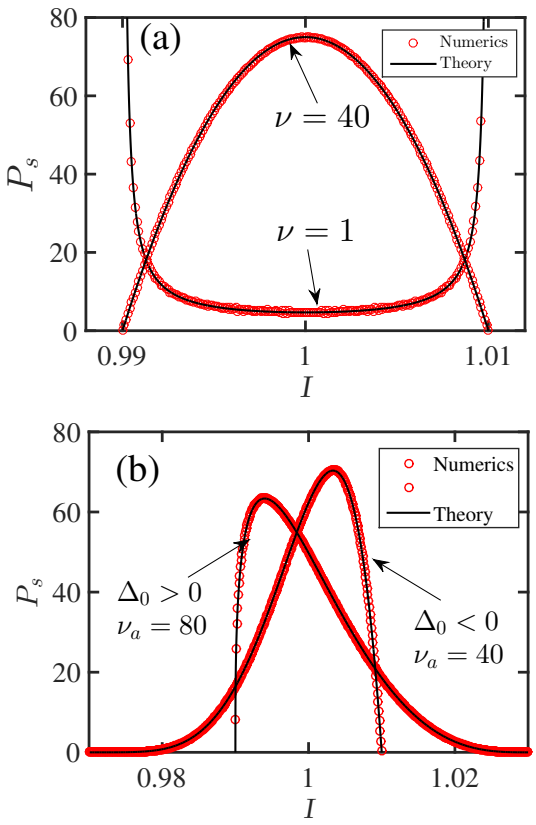

Fig. 8: (Color online) Theoretical (black solid lines) and numerical (red points) stationary probability distribution P_s as a function of electric current intensity I. (a) The symmetrical case with $a = b = 1$ for two parameter values $\nu = 1$ and $\nu = 40$. (b) The asymmetric case with parameters $a = 3$, $b = 1$, $\nu_a = 80$, and $a = 1$, $b = 3$, $\nu_a = 40$.

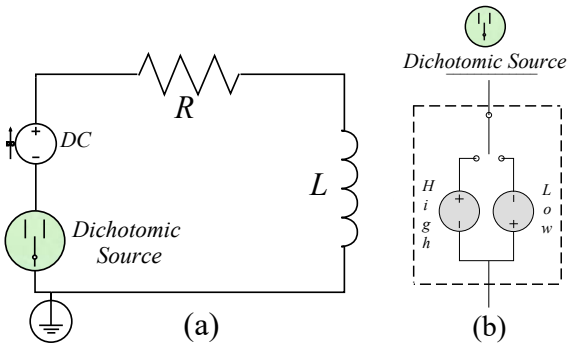

Fig. 9: (Color online) (a) Experimental setup. (b) Source of dichotomic alternating voltage

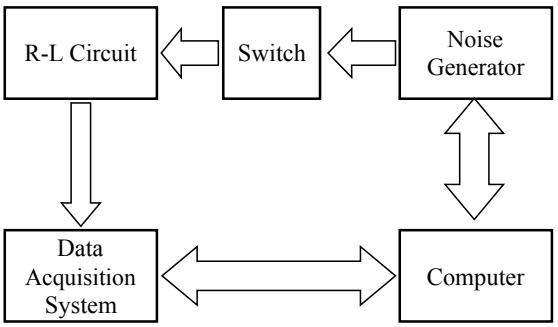

Fig. 10: Flow scheme of the proposed experiment.

part of next studies, however, computational simulations can be used to evaluate the different possibilities of a physical implementation.

The block diagram of the possible experimental setup is shown in Fig. 10. The dichotomous noise is generated using the seeds of the computer. This noise is used to trigger the switch control to the dichotomous source. The required data, like the instantaneous current in the circuit $I(t)$, the distribution of the electric current intensity along the experiments, and the stochastic noise generated by the seeds of the computer can be obtained with a digital acquisition system (DAQ).

7 Concluding remarks

We have found an exact analytical solution for the probability distribution function of an simple linear system driven by an asymmetric Markovian dichotomous noise. We studied the conditions under which the non-Maxwellian stationary probability distribution function exhibits a transition from a unimodal to a bimodal distribution. A phenomenon originally considered to be exclusive of non-linear SDEs.

The results show that the asymmetric dichotomous noise induces eight different behavior for the asymmetric probability distribution function $P_s(z)$ with respect to the average value of the variable $\langle z(t) \rangle$. This asymmetric behavior can be controlled by the parameters that define the dichotomous noise, i.e., a, b, and ν_a. It is noteworthy that the symmetric dichotomous noise only has access to two possible configurations for $P_s(z)$, which represent particular cases of the most general model introduced in this work.

Through the phase diagram, we discuss the eight different behaviors of the stationary probability distribution function and characterize them based on the asymmetry parameter Δ_0 and the inverse of the correlation time ν_a. When $\Delta_0 > 0$, we found three asymmetric distribution where its maximum is to the left of the mean value $\langle z(t) \rangle$ and on the contrary, if $\Delta_0 < 0$ we found three asymmetrical distribution where its maximum is on the right. For $\Delta = 0$, we recovered the symmetric case (see phase diagram) and the limit to Gaussian white noise. Results show a very good agree-

ment between the analytical equations and numerical simulations.

We explore possible applications in simple electronic circuits and in single species population growth models such as the Gompertz model. Finally, complex systems leading to bimodal distributions have been reported in the literature, our analytical results could contribute to the understanding of different systems, ranging from instabilities in plasmas, growth models [31] and noise in solid-state microstructures [41,43].

Acknowledgements MAGN thanks to project FONDECYT Regular 1201434 for financial support. R. Caicedo was financed in part by the Coordenação de Aperfeiçoamento de Pessoal de Nível Superior–Brasil (CAPES)–Finance Code 001.

Conflict of interest

The authors declare that they have no conflict of interest.

References

1. R.S. Oyarzabal, J.D. Szezech, A.M. Batista, J.M. Seoane, M.A. Sanjuán, Stochastic resonance in dissipative drift motion, Communications in Nonlinear Science and Numerical Simulation **54**, 62 (2018)
2. H. Calisto, F.R. Humire, Stochastic Resonance in Simple Electrical Circuits Driven by Quadratic Gaussian Noise, IEEE Transactions on Circuits and Systems II: Express Briefs **64**(8), 937 (2017)
3. W. Horsthemke, R. Lefever, *Noise induced transistions: Theory and Applications in Physics, Chemistry, and Biology*, Springer-Verlag, 2 ed., Berlin (2006)
4. V.V. Semenov, A.B. Neiman, T.E. Vadivasova, V.S. Anishchenko, Noise-induced transitions in a double-well oscillator with nonlinear dissipation, Physical Review E **93**(5), 1 (2016)
5. V.V. Semenov, Noise-induced transitions in a double-well excitable oscillator, Physical Review E **95**, 052205 (2017)
6. M. Bonnin, F. Corinto, S. Member, Phase Noise and Noise Induced Frequency Shift in Stochastic Nonlinear Oscillators, IEEE Transactions on Circuits and Systems—I: Regular Papers **60**(8), 2104 (2013)
7. M. Bonnin, F. Corinto, Influence of noise on the phase and amplitude of second-order oscillators, IEEE Transactions on Circuits and Systems II: Express Briefs **61**(3), 158 (2014)
8. C. Van Den Broeck, On the relation between white shot noise, Gaussian white noise, and the dichotomic Markov process, Journal of Statistical Physics **31**(3), 467 (1983)
9. A. Fulinski, Non-Markovian dichotomic noises, Acta Physica Polonica B **26**(6), 1131 (1995)
10. S.I. Denisov, W. Horsthemke, Mean first-passage time for an overdamped particle in a disordered force field, Physical Review E **62**(3), 3311 (2000)
11. T.T. Yang, H.Q. Zhang, Y. Xu, W. Xu, Stochastic resonance in coupled underdamped bistable systems driven by symmetric trichotomous noises, International Journal of Non-Linear Mechanics **67**, 42 (2014)
12. G. Kaniadakis, P. Quaratia, A set of stationary non-Maxwellian distributions, Physica A: Statistical Mechanics and its Applications **192**(4), 677 (1993)
13. W. Horsthemke, R. Lefever, Voltage-noise-induced transitions in electrically excitable membranes, Biophysical Journal **35**(2), 415 (1981)
14. M.A. Raadu, Effective distribution functions for electrostatic waves in dusty plasmas with a dust-size distribution, IEEE Transactions on Plasma Science **29**(2), 182 (2001)
15. M.O. Cáceres, Computing a non-Maxwellian velocity distribution from first principles, Physical Review E **67**(1), 016102 (2003)
16. O. Artime, A.F. Peralta, R. Toral, J.J. Ramasco, M. San Miguel, Aging-induced continuous phase transition, Physical Review E **98**(3), 1 (2018)
17. T. Biancalani, T. Rogers, A.J. McKane, Noise-induced metastability in biochemical networks, Physical Review E **86**(1), 1 (2012)
18. E. Jakeman, K.D. Ridley, Statistics of a filtered telegraph signal, J. Phys. A. Math. Gen. **32**(50), 8803 (1999)
19. J.M. Sancho, Stochastic processes driven by dichotomous Markov noise: Some exact dynamical results, Journal of Mathematical Physics **25**(2), 354 (1984)
20. R. Mankin, N. Lumi, Statistics of a leaky integrate-and-fire model of neurons driven by dichotomous noise, Physical Review E **93**(5), 1 (2016)
21. I. Bena, Dichotomous Markov noise: Exact results for out-of-equilibrium systems. A review, International Journal of Modern Physics B **20**(20), 2825 (2006)
22. J.E. Mazo, S.O. Rice, R.F. Pawula, On a Nonlinear Problem Involving RC Noise, IEEE Transactions on Information Theory **19**(4), 404 (1973)
23. L.D. Davisson, P. Papantoni-Kazakos, On the Distribution and Moments of RC-Filtered Hard-Limited RC-Filtered White Noise, IEEE Transactions on Information Theory **19**(4), 411 (1973)
24. W.M. Wonham, A.T. Fuller, Probability Densities of the Smoothed 'Random Telegraph Signal', Journal of Electronics and Control **4**(6), 567 (1958)
25. Narendra S. Goel, N. Richter-Dyn, *Stochastic models in biology*, 284, The Blackburn Press (2004)
26. C.W. Gardiner, *Handbook of Stochastic Methods: For Physics, Chemistry and Natural Sciences*, Springer-Verlag, 3 ed., Berlin (2004)
27. M. Wu, C.D. Andereck, Effects of External Noise on the Fréedericksz Transition in a Nematic Liquid Crystal, Physical Review Letters **65**(5), 591 (1990)
28. I. Browsell, I. L'Heureux, E. Fortin, Experimental evidence for dichotomous noise-induced states in a bistable interference filter, Physics Letters A **225**(2), 85 (1997)
29. E. Lazo, F.R. Humire, E. Saavedra, Disorder-order transitions in diluted and nondiluted direct transmissionlines with asymmetric dichotomous noise, International Journal of Modern Physics C **25**(7), 1 (2014)
30. D. Barik, P.K. Ghosh, D.S. Ray, Langevin dynamics with dichotomous noise; Direct simulation and applications, Journal of Statistical Mechanics: Theory and Experiment **03010**(3), P03010 (2006)
31. G. Aquino, M. Bologna, H. Calisto, An exact analytical solution for generalized growth models driven by a Markovian dichotomic noise, Europhysics Letters **89**(5), 50012 (2010)
32. V.E. Shapiro, V.M. Loginov, "Formulae of differentiation" and their use for solving stochastic equations, Physica A: Statistical Mechanics and its Applications **91**(3-4), 563 (1978)

33. N. Koshlyakov, M. Smirnov, E. Gliner, *Differential Equations of Mathematical Physics*, North-Holland Pub. Co., Amsterdam (1964)
34. W. Miller, Symmetries of Differential Equations. The Hypergeometric and Euler–Darboux Equations, SIAM Journal on Mathematical Analysis **4**(2), 314 (1973)
35. W.N. Bailey, *Generalized Hypergeometric Series*, Cambridge University Press (1964)
36. A.K. Laird, Dynamics of tumor growth, British Journal of Cancer **18**(3), 490 (1964)
37. C.F. Lo, Stochastic Gompertz model of tumour cell growth, Journal of Theoretical Biology, **248**, 317–321 (2007)
38. A. D'Onofrio, A. Fasano, B. Monechi, A generalization of Gompertz law compatible with the Gyllenberg-Webb theory for tumour growth, Mathematical Biosciences **230**(1), 45 (2011)
39. F.H. Hsieh, N.Z. Yen, Y.T. Juang, Optimal Controller of a Buck DC – DC Converter Using the Uncertain Load as Stochastic Noise, IEEE Transactions on Circuits and Systems II: Express Briefs **52**(2), 77 (2005)
40. S.K. Magierowski, S. Zukotynski, CMOS LC -Oscillator Phase-Noise, IEEE Trans. Circuits Syst. I Regular Papers **51**(4), 664 (2004)
41. A.P. Van Der Wel, E.A.M. Klumperink, J.S. Kolhatkar, E. Hoekstra, M.F. Snoeij, C. Salm, H. Wallinga, B. Nauta, Low-frequency noise phenomena in switched MOSFETs, IEEE Journal of Solid-State Circuits **42**(3), 540 (2007)
42. A. Grebennikov, High-Efficiency Class-E Power Amplifier with Shunt Capacitance and Shunt Filter, IEEE Transactions on Circuits and Systems I: Regular Papers **63**(1), 12 (2016)
43. M.J. Kirton, M.J. Uren, Noise in solid-state microstructures: A new perspective on individual defects, interface states and low-frequency (1/f) noise, Advances in Physics **38**(4), 367 (1989)

Figures

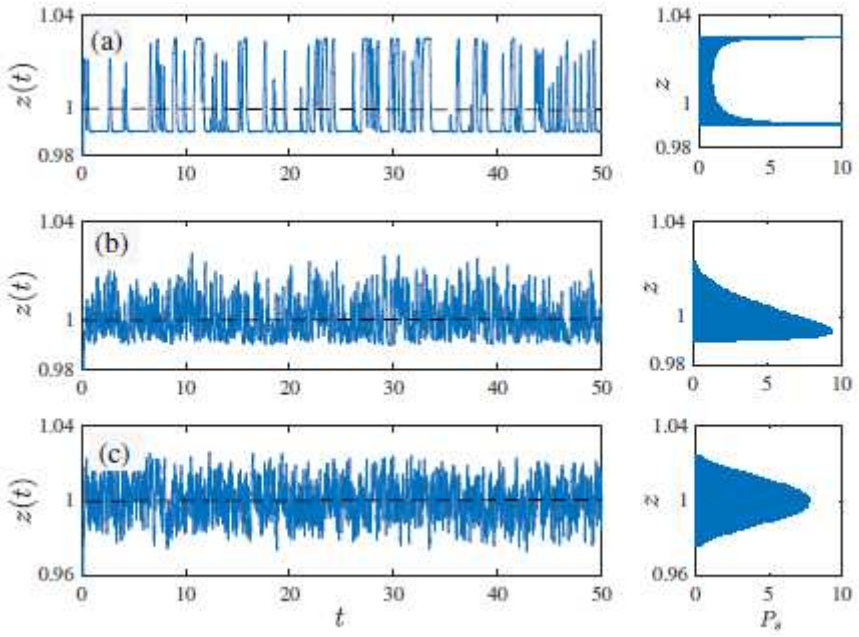

Figure 1

See manuscript for full figure caption.

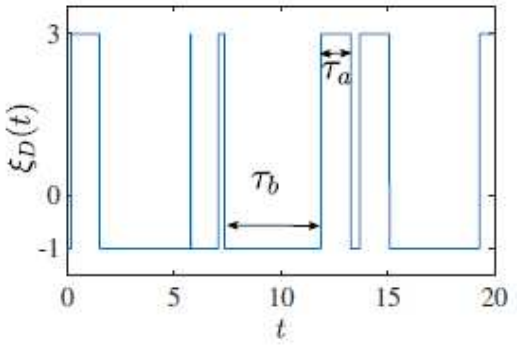

(a) The asymmetric case considering the values $a = 3$, $b = 1$, $\nu_a = 1$, and $\nu_b = 1/3$.

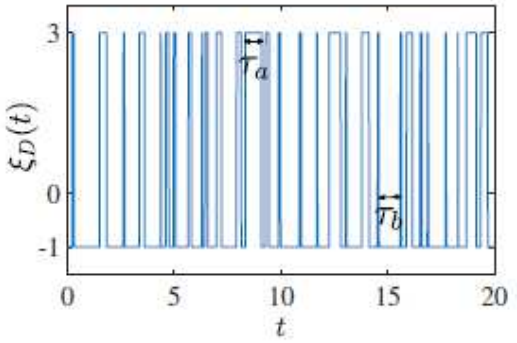

(b) The asymmetric case considering the values $a = 3$, $b = 1$, $\nu_a = 6$, and $\nu_b = 2$.

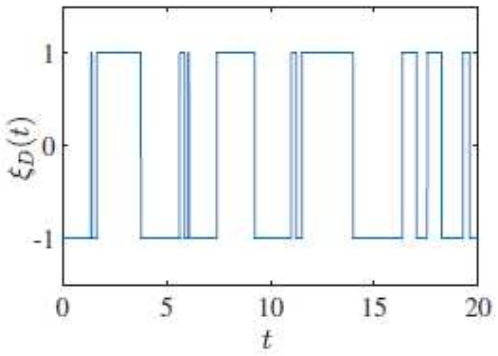

(c) The symmetric case considering the values $a = b = 1$ and $\nu_a = \nu_b = \nu = 1$.

Figure 2

See manuscript for full figure caption.

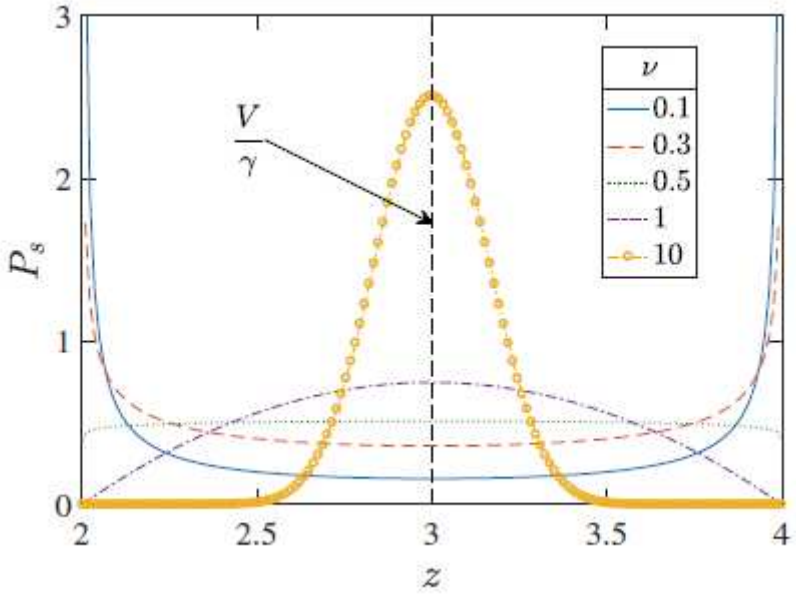

Figure 3

See manuscript for full figure caption.

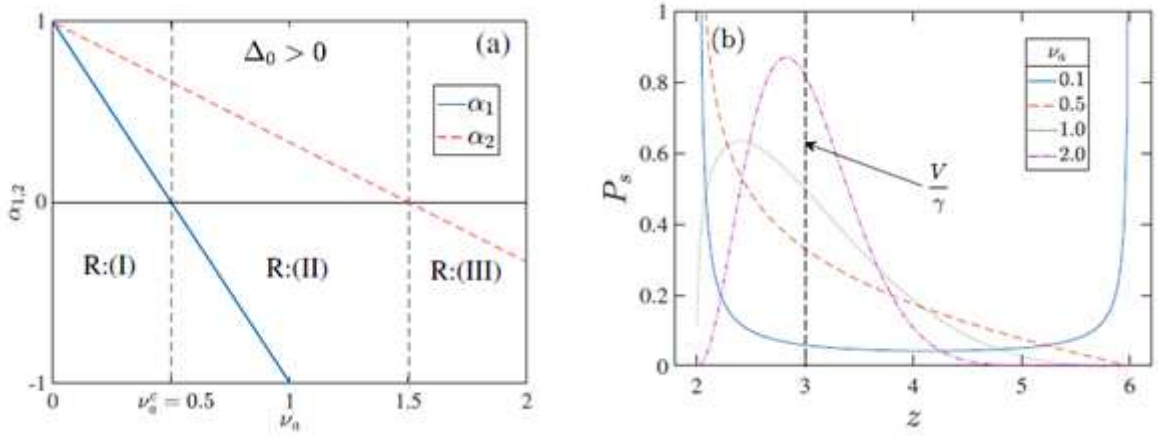

Figure 4

See manuscript for full figure caption.

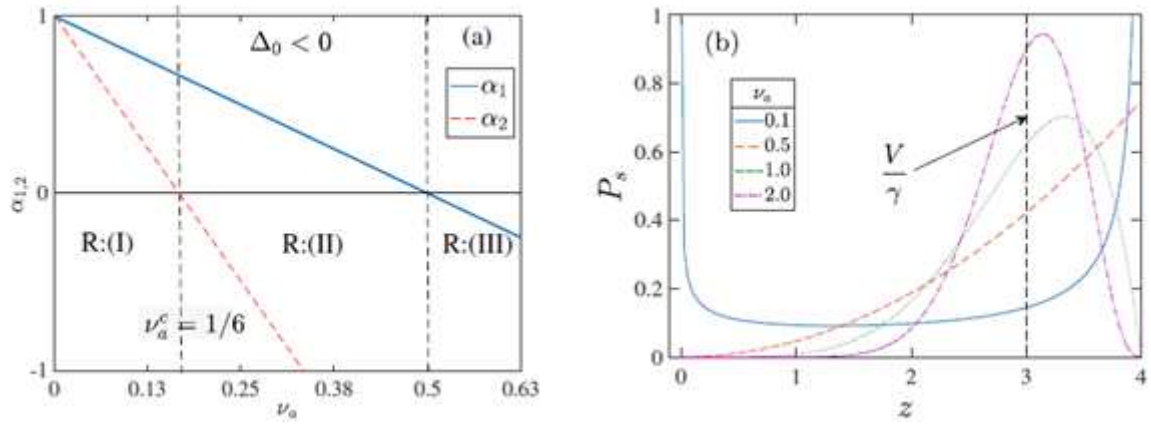

Figure 5

See manuscript for full figure caption.

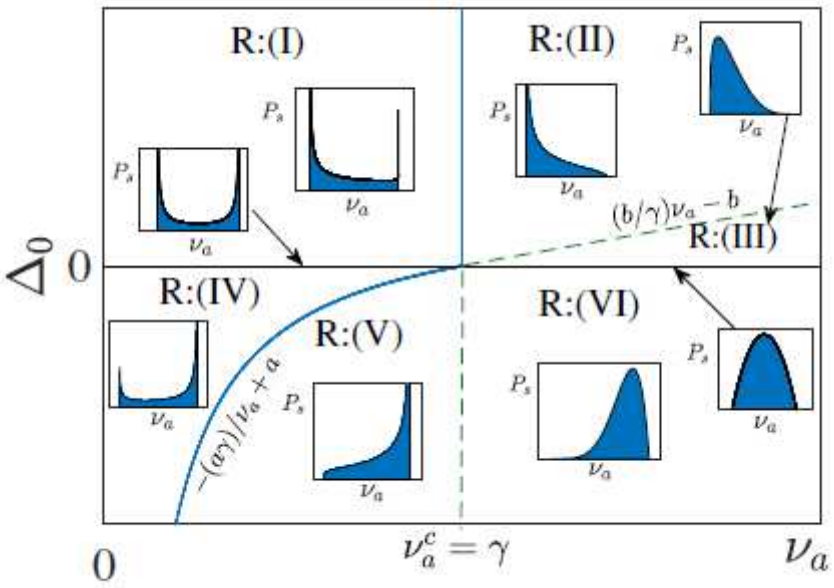

Figure 6

See manuscript for full figure caption.

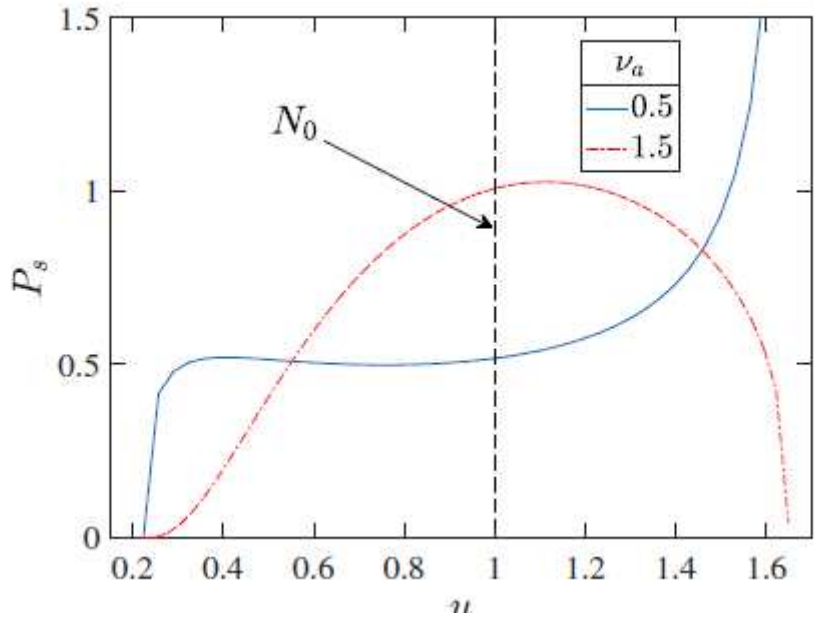

Figure 7

See manuscript for full figure caption.

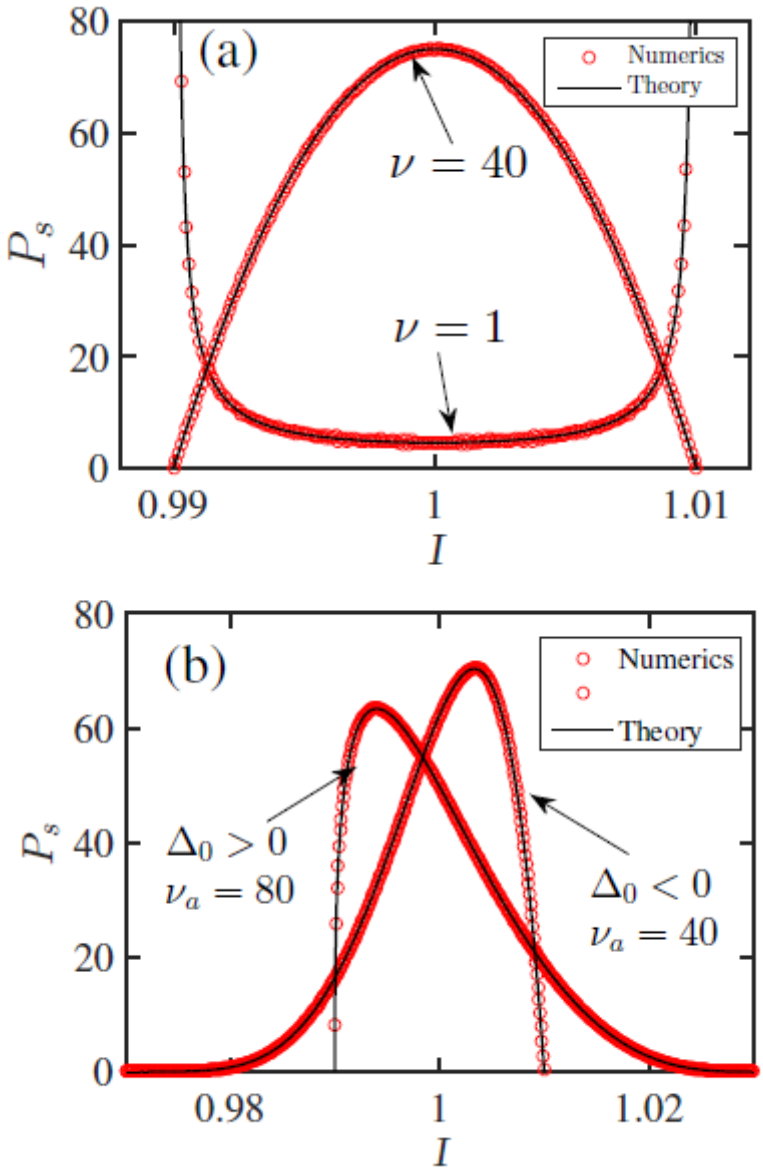

Figure 8

See manuscript for full figure caption.

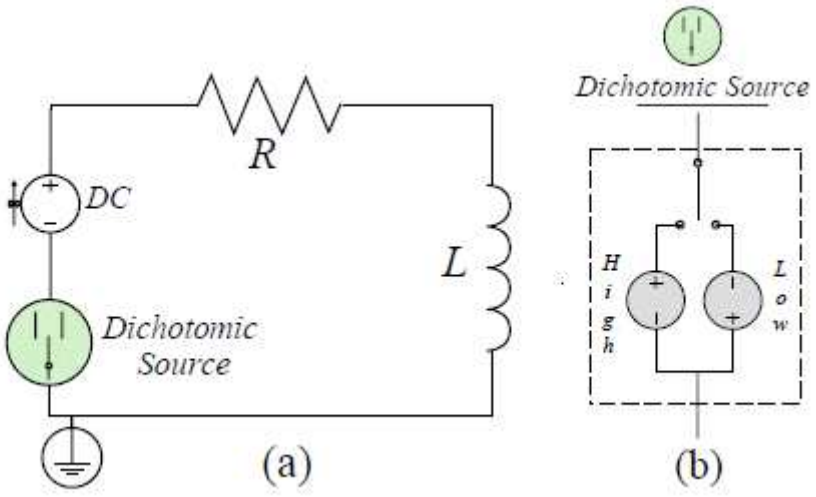

Figure 9

See manuscript for full figure caption.

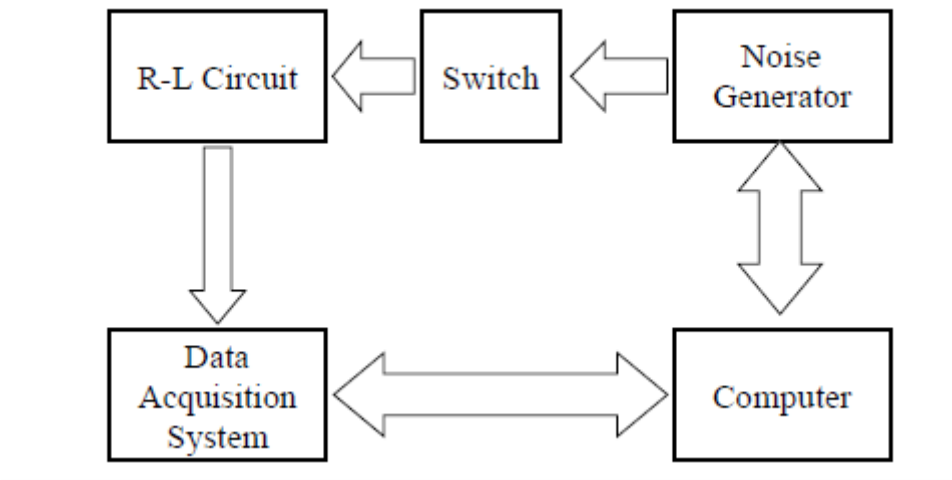

Figure 10

See manuscript for full figure caption.